Structured Robust Control for the Aerodynamic Steering of Reusable Rockets ⋆

Marco Sagliano * **Stefano Farì** * **José Macés Hernandéz** *
Ansgar Heidecker * **José Garrido** * **Matthias Winter** *
David Seelbinder * **Markus Schlotterer** * **Svenja Woicke** *
Etienne Dumont *

* *German Aerospace Center, Robert Hooke Str. 7, 28359, Germany (e-mail: name.surname@ dlr.de).*

Abstract: This paper investigates the use of structured H_∞ control for the aerodynamic descent phase of a reusable rocket. A unified control strategy for attitude and position is proposed and verified. The architecture of the controller, together with the observed performance are discussed. Results are presented for CALLISTO, a reusable rocket demonstrator jointly developed by DLR, JAXA and CNES.

Keywords: Structured H_∞ , Robust Control, Reusable Rockets, Aeroydnamic Descent, CALLISTO

1. INTRODUCTION

December, 21, 2015 marked the formal beginning of the reusability era for rockets at industrial level. On that date SpaceX showed that it was possible to reuse commercial launcher systems by landing its Falcon 9 first stage after having put a payload into orbit. Elon Musk's company has undoubtedly demonstrated that the reusability paradigm is now at our hand (space.com [2015]). Other companies like Rocket Lab are following a similar path with the development of the reusable rocket Neutron (Rocket Lab [2021]). Consequently, space agencies are reshaping their strategies, and embracing the reusability paradigm shift. With this long-term perspective in mind and the aim to develop strategic technologies in the frame of a wider reusability-focused program the German Aerospace Center (DLR), the Japan Aerospace Exploration Agency (JAXA), and the French National Centre for Space Studies (CNES) decided to share know-how, resources and efforts to develop and demonstrate the technologies that will be needed for future reusable launch vehicles. The result of such cooperation is the CALLISTO (Cooperative Action Leading to Launcher Innovation in Stage Toss back Operations) project: a demonstrator for a reusable vertical take-off, vertical landing rocket, acting as first stage. CALLISTO aims at paving the way to the first European/Japanese reusable rocket that will perform its first flights from the Kourou Space Center (KSC), in French Guiana.

While the rocket and most of its components are jointly developed by the three agencies, two separated G&C (Guidance and Control) subsystems are developed in parallel: a CNES-led one, and a DLR-JAXA fully integrated G&C subsystem. This choice allows to test dedicated G&C systems developed independently while enjoying the benefits coming from the joint efforts of having a unique demonstrator. CALLISTO will be employed over several flights of increasing complexity, each of them consisting of multiple phases. For what regards the last flight class, i.e., the demo mission, four phases are foreseen: the ascent, the boostback, the aerodynamic descent and the powered landing. In this paper we focus on the control strategy for the aerodynamic descent phase: the control system in fact is in charge of counteracting disturbances and uncertainties acting on the vehicle while satisfying the strict accuracy requirements needed to realize the pinpoint landing during the subsequent powered phase.

A very elegant and appealing solution to the control problem with guaranteed stability margins is represented by the H_∞ family of methods proposed by Glover and Doyle (Glover and Doyle [1988]). These methods overcome the drawback in terms of classical margins of linear quadratic Gaussian (LQG) regulators, highlighted by Doyle in his famous paper, where he realized that "There are none" (Doyle [1978]). This intuition led to the development of the H_∞ framework for Linear-Time-Invariant (LTI) systems, residing in the frequency-wise minimization of the maximum gain that a given output will experience for a unitary excitation of a generalized exogenous input. The framework takes advantage of Linear Fractional Transformations (LFTs) to include the feedback action in the loop (Doyle et al. [1991]). This methodology has been very successful, since it allows to incorporate frequency-domain requirements in the design process. The synthesis is performed by choosing weighting functions to emphasize a given objective within a specific range of frequencies, and the entire process is nowadays highly automatized through the popular Matlab's *hinfsyn* routine. The main drawback of this methodology is that the computed controller is an LTI whose size is at least as large as the size of the augmented plant itself. Clearly, this rapidly leads to a large increase of the size of the controller, and

⋆ The first author thanks DLR for providing special funding for his stay in Japan in the frame of the CALLISTO joint work, JAXA for providing hosting, Dr. Andrés Marcos and Dr. Diego Navarro-Tapia for the several fruitful discussions on structured robust control, and the anonymous reviewers for their useful comments.

consequently to the need of applying ad-hoc reduction techniques (with a potential performance decrease). The aforementioned limitation has been mitigated by the second generation of H_∞ methods, the so-called *structured* H_∞ techniques (Apkarian and Noll [2006a]). Differently from the full H_∞ methods, in the structured synthesis the designer imposes a specific control template, like a Proportional-Integral-Derivative (PID), or an LTI system with a defined number of states. The routine translates the template specifications into a set of constraints that leads to a non-smooth, non-convex optimization problem rather than to a non-smooth, convex one as for the original H_∞ problem. Despite the more complex mathematical framework, the procedure is fully automatized through the command *hinfstruct*, used throughout this work, and that performs very well in practice.

From the point of view of the applications the aforementioned methodology has found significant applications in the space sector, especially in the launchers segment. It is a technology studied both in the United States for the development of the Ares I system (that later evolved into the Space Launch System program) (Wie et al. [2008]), and in Europe for the Ariane-class rockets (Knoblauch et al. [2012]). An interesting case is represented by the application of structured H_∞ techniques to the VEGA launcher (Navarro-Tapia et al. [2019], Navarro-Tapia [2019]). It is worth noticing that while this topic is getting more and more explored for the ascent phase, still, despite some remarkable exceptions (Simplicio et al. [2019]) the properties of the same methodology for the descent phase of a reusable rocket remain largely unexplored.

This paper extends our previous work (Sagliano et al. [2021]), where a classic cascade of loops was considered. In this work we merge the loops into a unified controller for trajectory tracking through the active use of fin deflections. The organization of this paper is the following: in Sec. 2 we define the control problem for the aerodynamic descent phase. We describe the formulation of the H_∞ problem in Sec. 3, and analyze it in Sec. 4. Finally, some conclusions regarding the work performed are drawn in Sec. 5.

2. PROBLEM STATEMENT

This section describes the aerodynamic descent phase of CALLISTO. Note that the formulation can be extended to any reusable rocket. We focus on the vehicle and the mission profiles, and then we describe the equations of motion used to model the dynamics of CALLISTO.

2.1 Vehicle and Mission Description

CALLISTO has a Liquid-Hydrogen (LH2) - Liquid Oxigen (LOX) engine, able to generate a thrust in the order of 40 kN. Its throttling capability can vary from 40% to more than 100%. The demonstrator is about 13 m tall, with a diameter of about 1 m. The engine is mounted on a gimballed system to allow to control the thrust vector pointing direction. During the active propulsion phases this guarantees full pitch and yaw control capability. The roll control is realized mainly through a set of Reaction-Control System (RCS) thrusters, which are installed at the top of the vehicle. During the non-propelled phases three-axes control is achieved through a set of four aerodynamic fins which are mounted in a "+" configuration. Control-wise these 4 physical fins are mapped onto an equivalent set of 3 *virtual fins* δ_ϕ, δ_θ, δ_ψ, which are used to express the aerodynamic coefficients with respect to the three possible rotations, and therefore, are actively used for the formulation of the equations of motion. Finally, CALLISTO mounts a set of 4 foldable legs able to absorb the touchdown shock and ensure proper stabilization of the rocket once the landing event occurs. An impression of the vehicle is shown in Fig. 1, together with its body axes, centered in the Center of Mass (CoM) of the rocket. Note

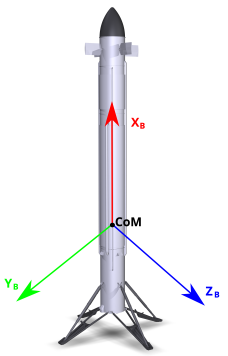

Fig. 1. CALLISTO experimental vehicle

that whereas we refer to the CALLISTO demonstrator throughout this work the problem and the formulation can be considered applicable to the aerodynamic descent of any reusable rocket having a set of fins for aerodynamic control. This broad range of vehicles can potentially include vehicles like SpaceX's Falcon 9 and Rocket Lab's Neutron.

For what regards the mission profile the flight will take place in French Guiana, at the Guiana Space Centre (GSC). After the ascent phase the vehicle starts its boostback maneuver to invert the direction of the velocity vector. After this maneuver is complete a Main Engine Cut Off (MECO) command is issued, and the vehicle starts its unpowered descent. As soon as the dynamic pressure is strong enough the actively-controlled aerodynamic descent begins. In this phase the attitude control is ensured by the fins that will steer the vehicle such that a given aerodynamic force, needed to track the trajectory, is generated. The aerodynamic control phase is concluded at a specific altitude, where the engine is then re-ignited and the powered descent and landing phase begins. The reference trajectory provided by CNES, computed with multi-phase optimization techniques, and showing the difference phases of flight can be seen in Fig. 2.

2.2 6-DoF Equations of Motion

The mathematical description of the equations of motion relies upon a target-centered reference frame, whose axes are aligned with the downrange and crossrange (DCA) main directions, and the reference frame is centered at the landing position. Consequently we refer to this choice as *DCA reference frame*. This selection is beneficial as it makes the decoupling of the longitudinal and lateral control channels easier, which are dominated by pitch and yaw, (and named accordingly), and here considered

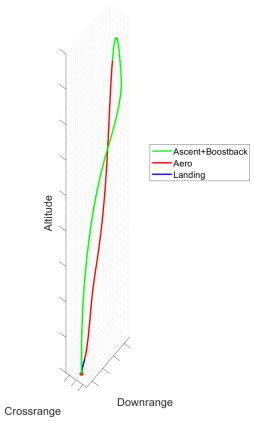

Fig. 2. CALLISTO reference trajectory

separately. With these premises we can formulate the unpowered 6-DOF motion of a reusable rocket as

$$\begin{aligned}\dot{\mathbf{r}} &= \mathbf{v}\\ \dot{\mathbf{v}} &= \mathbf{a}^{grav} + \mathbf{a}^{aero} + \mathbf{a}^{fict}\\ \dot{\phi} &= p + (q\sin\phi + r\cos\phi)\tan\theta\\ \dot{\theta} &= q\cos\phi - r\sin\phi\\ \dot{\psi} &= (q\sin\phi + r\cos\phi)\cos\theta^{-1}\\ \dot{\omega} &= \mathbf{I}^{-1}\left(\mathbf{M}^{aero} - \omega\times(\mathbf{I}\cdot\omega)\right)\end{aligned} \tag{1}$$

where $\mathbf{r}$ and $\mathbf{v}$ are the position and velocity of the CoM of the vehicle expressed in the DCA reference frame. The attitude is represented as a set of Euler angles $\mathbf{ea} = [\phi \quad \theta \quad \psi]^T$, equal to 0 when the body axes are aligned with the Up, Crossrange and Downrange directions. This choice allows to avoid singularities when the vehicle is moving vertically, and is therefore a suitable solution for the descent and landing phase. $\mathbf{I}$ is the inertia matrix of CALLISTO, here assumed constant, whereas the terms $\mathbf{a}^{grav}$, $\mathbf{a}^{aero}$ and $\mathbf{a}^{fict}$ represent the gravitational, aerodynamic and fictitious (i.e., Earth-rotation related) accelerations acting on the rocket, respectively. They are computed as

$$\begin{aligned}\mathbf{a}^{grav} &= -\mu_{\oplus}\frac{\mathbf{r}+\mathbf{r_L}}{\|\mathbf{r}+\mathbf{r_L}\|^3}\\ \mathbf{a}^{aero} &= \mathbf{R}_B^{DCA}\cdot\tfrac{1}{2}\rho V^2 A_{ref}/m\,[C_x \quad C_y \quad C_z]^T\\ \mathbf{a}^{fict} &= -2\omega_{\oplus}\times\mathbf{v} - \omega_{\oplus}\times(\omega_{\oplus}\times\mathbf{r})\end{aligned} \tag{2}$$

with $\mathbf{r}_L$ the position vector of the landing position with respect to the center of the Earth, m is the mass of CALLISTO, the rotation matrix $\mathbf{R}_B^{DCA}$ representing the transformation from Body to the DCA axes and given by Eq. (3). The inverse transformation is computed by using the transpose of $\mathbf{R}_B^{DCA}$, since the inverse and the transpose of a rotation matrix coincide. The angular rates $\omega = [p \quad q \quad r]^T$ depend on the aerodynamic torque $\mathbf{M}^{aero}$ as follows:

$$\mathbf{M}^{aero} = \frac{1}{2}\rho V^2 A_{ref} L_{ref}/m\,[C_l \quad C_m \quad C_n]^T \tag{4}$$

The aerodynamic coefficients

$$C_x, C_y, C_z, C_l, C_m, C_n \tag{5}$$

refer to the body's CoM, and depend on the Mach number M, the angle of attack α, the side-slip angle β (which embed the attitude information) and the virtual fin deflections δ_ϕ, δ_θ and δ_ψ, while ρ and V refer to the atmospheric density and the speed, respectively. They are computed with CFD techniques, and validated with wind-tunnel tests (Marwege et al. [2019]). A_{ref} and L_{ref} are the reference area and the reference length of the rocket.

With this formulation we can derive the control scheme, where the reference values of $\mathbf{r}$, $\mathbf{v}$, $\mathbf{ea}$, and ω are compared with the actual ones and used by the controller to determine the control action directly in terms of virtual fin deflections variations $\delta\phi$, $\delta\theta$, and $\delta\psi$, as shown in Fig. 3. In the next sections we will show some of the results obtained by using the structured H_∞ framework applied to this formulation of the equations of motion.

3. $\mathbf{H}_\infty$ SYNTHESIS

3.1 Overall architecture

In the classical H_∞ theory the synthesis process is embedded into a convex optimization problem, and the resulting controller is a transfer function having at least the same order of the augmented plant to be controlled (Gahinet and Apkarian [1994]). However, the resulting controller might be difficult to implement on a real system in case it shows high-frequency poles. Moreover, the industrial adoption of controllers based on high-order transfer functions is generally less straightforward (Navarro-Tapia [2019]). The framework developed by Apkarian and Noll is based on non-smooth optimization techniques to include the constraints representing the template definition in the H_∞ synthesis (Apkarian and Noll [2006b]). Therefore, it becomes possible to re-introduce classical control structures such as PIDs, which are easier to understand and verify with industrial standards. In CALLISTO we propose to formulate the control problem by unifying trajectory and attitude control for the pitch and yaw channels. Namely, the pitch controller will take care of the downrange position and velocity as well as the pitch angle and the q component of the angular rate vector. Conversely, the yaw controller will take care of the crossrange position and velocity, together with the yaw angle and the r component of the angular rate vector. The only difference is represented by roll, having its own controller, taking care of the roll angle ϕ and the p component of ω. The procedure to derive the controller comprises the following steps:

(1) Define the number of operating points for which a controller is to be synthesized.
(2) Choose a monotonically changing variable to be used as a scheduling parameter. For this work the altitude has been selected.
(3) Sample the states and controls of the reference trajectory along the scheduling parameter.
(4) Perform an analytical linearization of the equations of motion of Eq. (1) to come up with a series of LTI systems.
(5) Perform a control synthesis and analysis for each of the LTIs obtained.
(6) Analyze the individual linear controllers in both frequency and time domain.
(7) Implement the gain-scheduling nonlinear controller by linearly interpolating the different gain matrices based on the current altitude.

$$\mathbf{R}_B^{DCA} = \begin{bmatrix} \cos\theta\cos\psi & \sin\phi\sin\theta\cos\psi - \cos\phi\sin\psi & \cos\phi\sin\theta\cos\psi + \sin\phi\sin\psi \\ \cos\theta\sin\psi & \sin\phi\sin\theta\sin\psi + \cos\phi\cos\theta & \cos\phi\sin\theta\sin\psi - \sin\phi\cos\psi \\ -\sin\theta & \sin\phi\cos\theta & \cos\phi\cos\theta \end{bmatrix} \tag{3}$$

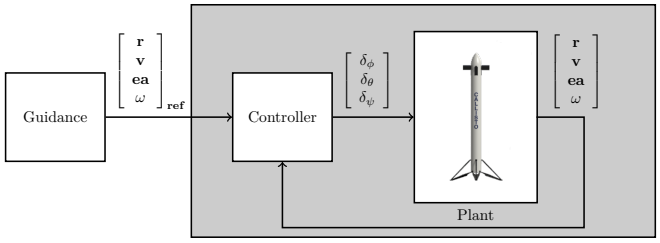

Fig. 3. CALLISTO control loop for the aerodynamic descent

3.2 Roll control

For the synthesis of roll control with the structured H_∞ framework we derived the augmented plant P represented in Fig. 4. The exogenous inputs are the reference signal r, scaled by a constant weighting function W_{ref}, which translate into the physical roll signal ϕ_{ref}, and the angular rate p_{ref}. We have a corresponding noise signal n, scaled by W_n, that leads to the physical signals n_ϕ, n_p, which, combined with the plant outputs, form the measurement signals ϕ_m, p_m. The comparison of the reference and the measured signals generate the errors e_ϕ, e_p entering the controller K. The outcome is the roll-related deflection command $\delta_{\phi,cmd}$. An error on the input deflection $\delta_{phi,d}$ is also considered, so the total deflection will be given by their sum $\delta_{\phi,tot}$. This is the signal that physically interacts with the plant G_ϕ. For the tuning of the system we employ a mixed $T/S/KS$ sensitivity approach, where the sensitivity transfer functions T, S and KS shape the tracking performance, the error performance, and the control efforts, respectively. The roll controller has the form

$$K(s) \triangleq \left(\frac{k_i}{s} + k_p\right) e_\phi + k_d e_p \tag{6}$$

and the purpose of the optimization is therefore to

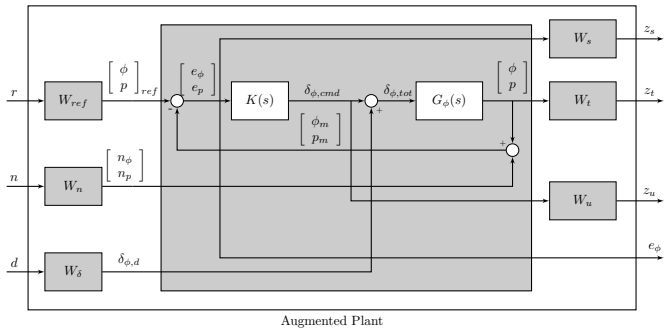

Fig. 4. Roll Control augmented plant

minimize γ as follows,

$$\underset{k_i,k_p,k_d}{\text{minimize}}\ \gamma = \left\| P_{\mathbf{r}\to\mathbf{z}(s)} \right\|_\infty \tag{7}$$

where the vectors $\mathbf{r}$ and $\mathbf{z}$ are given by Eq. (8).

$$\mathbf{r} \triangleq \begin{bmatrix} r \\ n \\ d \end{bmatrix},\ \mathbf{z} \triangleq \begin{bmatrix} z_s \\ z_t \\ z_u \end{bmatrix} \tag{8}$$

The optimizer determines the gains k_p, k_d, k_i associated with a PID-like control structure which minimize the ∞-norm of the transfer function from $\mathbf{r}$ to $\mathbf{z}$ while stabilizing the closed loop.

3.3 Pitch and Yaw control

The same process is repeated for pitch and yaw (here depicted only for the pitch dynamics in Fig. 5, given the strong similarity with the yaw results). Here we use the downrange position and velocity D and v_D, in addition to the pitch angle θ and the body angular rate q. We

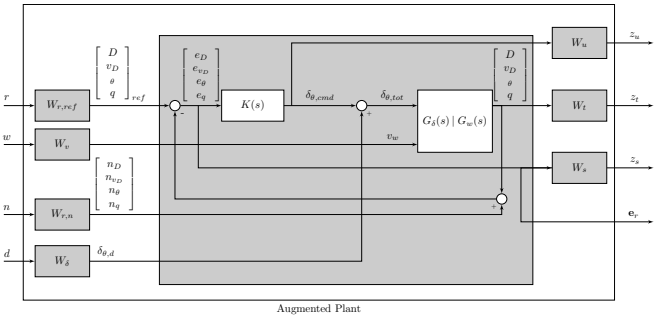

Fig. 5. Trajectory Tracking control augmented plant

can observe three main differences with respect to the roll: 1) the trajectory tracking and the attitude control are unified. The attitude channel no longer has its own loop as in (Sagliano et al. [2021]), but serves directly as means of control for the trajectory tracking purposes. The consequence is that the baseline plant (i.e., excluding actuator dynamics and delays) is no longer made of a pair of second-order systems, but a unique fourth-order system. 2) the unification results into a different control law: since we have position and attitude measurements, the following control law is used.

$$K(s) \triangleq \left(\frac{k_{i,z}}{s} + k_{p,z}\right) e_D + k_{p,v_d} e_{vD} + k_{p,\theta} e_\theta + k_{d,p} e_q \tag{9}$$

Note that this control law mimics the idea proposed for launchers (Navarro-Tapia [2019]) with the fundamental difference that, to obtain zero steady-state errors, we introduce an integrator as well. This choice allows to reduce the gap with full H_∞ controllers, while having a minimum impact on the complexity of the control structure. 3) while wind was only considered in the nonlinear simulations in our aforementioned work, we explicitly consider it as an exogenous input in the pitch dynamics. The consequence is that wind effects can be analyzed also with linear-analysis tools. We also highlight a note regarding the input disturbance term d: this unitary signal is scaled by a constant function W_d, representing the magnitude of the real disturbances $\delta_{\theta,dist}$, which will modify the real deflection δ_θ generated by the actuator, leading to the final value $\delta_{\theta,tot}$. Especially for pitch and yaw the use of this term is two-fold beneficial: on one hand, it allows to include errors in the commanded deflections, coming for instance from servo-actuators steady-state errors. On the other hand, its

inclusion avoids undesired zero-pole cancellation (Werner [2014]). The synthesis problem is therefore posed as

$$\underset{k_{i,z},k_{p,z},k_{d,z},k_{p,\theta},k_{d,p}}{\text{minimize}} \quad \gamma = \left\| P_{\mathbf{r}\to\mathbf{z}(s)} \right\|_\infty \tag{10}$$

where the vectors $\mathbf{r}$ and $\mathbf{z}$ are now defined as follows.

$$\mathbf{r} \triangleq \begin{bmatrix} r \\ w \\ n \\ d \end{bmatrix}, \ \mathbf{z} \triangleq \begin{bmatrix} z_t \\ z_s \\ z_u \end{bmatrix} \tag{11}$$

Note that, as aforementioned, for the yaw control the same process as for the pitch has been implemented. Therefore, the scheme is here omitted for avoiding redundant information. Finally, all the weighting functions are built as

$$W \triangleq \frac{s + \omega_s l_s}{s/h_s + \omega_s} \tag{12}$$

where the terms h_s and l_s represent the desired high-frequency and low-frequency asymptotes of the weighting function, while ω_s is the approximated cross-frequency. The different values of h_s, l_s and ω_s depend on whether they refer to the complementary sensitivities W_t, the sensitivities W_s, or the control sensitivities W_u. For instance, the weight associated with the sensitivity transfer function is built as a low-pass filter, while the one associated with the complementary sensitivity is a high-pass filter. Finally, note that the presence of z_t in both the roll and pitch/yaw design has only the purpose of limiting the closed-loop bandwidth, and plays a minor role in the design. Even if it could be excluded from the design, this term provides a further knob for control fine-tuning Navarro-Tapia [2019], and is therefore kept in the current formulation.

3.4 Gain Scheduling

Similarly to what done in our previous work (Sagliano et al. [2021]) we sample the system along the reference trajectory in n different points (with $n = 15$ in this case), leading to a corresponding number of LTI systems. The nonlinear control law is obtained by interpolating the gains linearly as follows,

$$k(h) = k_{i-1} + (k_i - k_{i-1}) \frac{h - h_{i-1}}{h_i - h_{i-1}}, \quad \begin{matrix} h \in [h_{i-1}, h_i] \\ i = 2, \ldots, n \end{matrix} \tag{13}$$

where k represents in general form any of the gains of Eqs. (6),(9), and h is the geodetic altitude. Although the choice of this scheme implies that the synthesized LTI controllers will only be used pointwise at the individual h_i the similarity of consecutive plants is such that no sudden jumps are experienced along the trajectories, leading to an overall smooth nonlinear feedback control action.

4. LINEAR ANALYSIS AND CLOSED-LOOP VALIDATION

This section shows some of the linear analysis results obtained by applying the procedure highlighted in Sec. 3. First we present the frequency-domain results for the roll controller: the Nichols chart is depicted in Fig. 6, whereas the sensitivity is shown in Fig. 7. From the Nichols plot in Fig. 6 we can see that no instabilities are observed for any of the synthesized controllers. The minimum stability margins are equal to 12 dB and 55 deg in terms of gain and phase, respectively. The sensitivity transfer function confirms this results, since no significant peaks are present, and good tracking properties are observed at low frequencies. Similar observations can be made

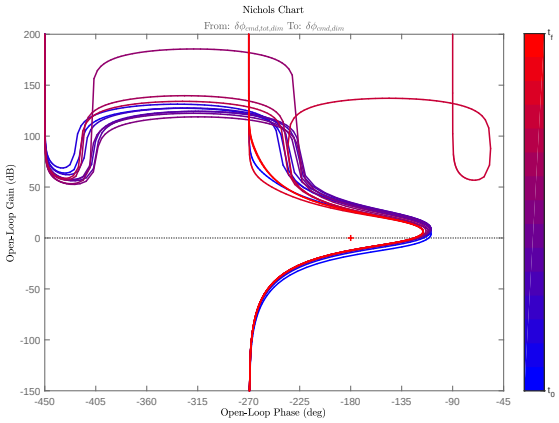

Fig. 6. Nichols chart for the roll controller.

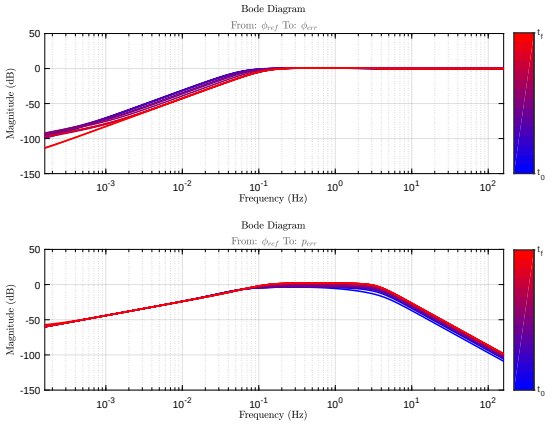

Fig. 7. Sensitivity for the roll controller.

for the pitch: specifically, from the Nichols plots in Fig. 8 it is possible to see that the minimum gain margin is equal to about 10 dB, with a minimum phase margin of 47 deg. In all the cases we are above the requirements established for CALLISTO. These results confirm that the methodology is able to provide a very robust control law able to tolerate uncertainties and time delays. Also in terms of sensitivity transfer function (Fig. 9) no peaks in frequency are observed, and good tracking performance can be seen. These conclusions are confirmed by the time-domain results (here omitted).

These results are valid for nominal conditions, i.e., no uncertainties are included in the formulation, although this can be easily done with the structured H_∞ framework. Finally, we tested the overall controller within the 6-DoF nonlinear closed-loop environment to verify that the control strategy was effectively able to control the real plant in presence of multiple uncertainties and disturbances. Results showing the errors in terms of position and velocity for a Monte-Carlo campaign of 100 cases are depicted in Fig. 10. These results confirm that the system is stable and the controller able to manage the errors along the entire aerodynamic phase for all the cases.

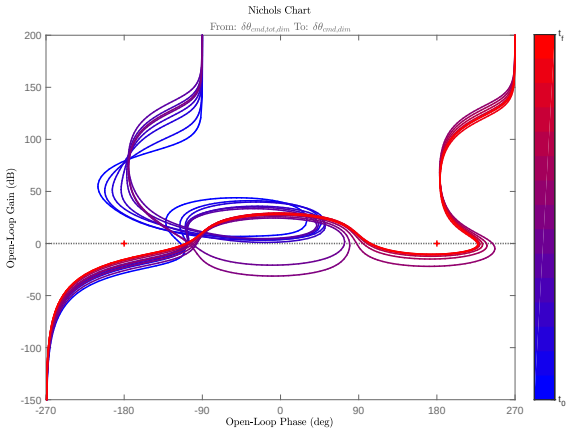

Fig. 8. Nichols chart for the pitch controller.

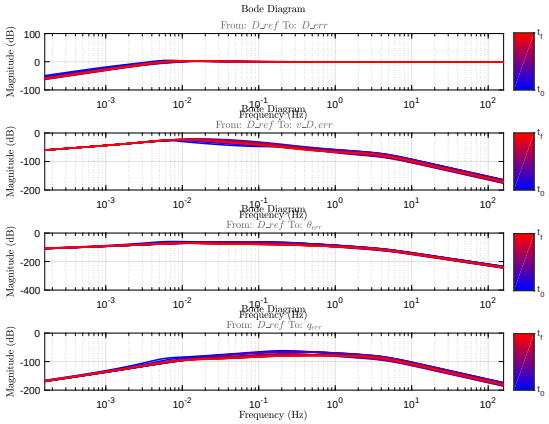

Fig. 9. Sensitivity for the pitch controller.

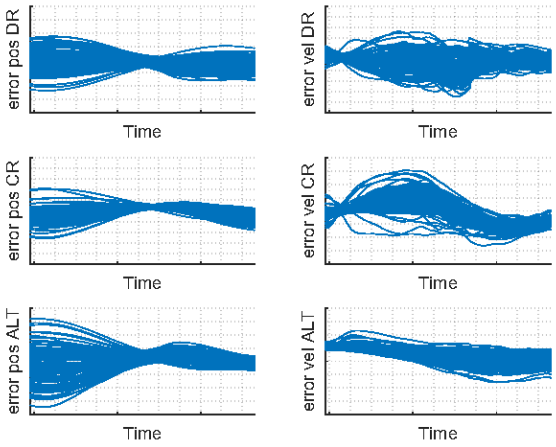

Fig. 10. Monte-Carlo preliminary results for the nonlinear plant in presence of disturbances.

5. CONCLUSIONS

In this paper we proposed a structured H_∞ controller for the aerodynamic phase of reusable rockets. Moving beyond the classical outer loop / inner loop cascade control design, we unified the control structure for pitch and yaw through an augmented PID-like control law, whereas for roll control a simpler PID-like template was adopted. Results in terms of Nichols plots, and sensitivity transfer functions confirm the validity of the approach, making the proposed structured H_∞ control synthesis a valid candidate for the real flight of the CALLISTO demonstrator.

Further development will focus on the inclusion of uncertainties and delays in the design, and on a more formal and thorough robustness analysis, for instance in terms of plant/controller mismatch representing non-perfect scheduling conditions.

REFERENCES

Apkarian, P. and Noll, D. (2006a). Frequency domain h_∞ synthesis using nonsmooth techniques. In *2006 1ST IEEE Conference on Industrial Electronics and Applications*. IEEE. doi:10.1109/iciea.2006.257082.

Apkarian, P. and Noll, D. (2006b). Nonsmooth h∞synthesis. *IEEE Transactions on Automatic Control*, 51(1), 71–86. doi:10.1109/tac.2005.860290.

Doyle, J. (1978). Guaranteed margins for LQG regulators. *IEEE Transactions on Automatic Control*, 23(4), 756–757. doi:10.1109/tac.1978.1101812.

Doyle, J., Packard, A., and Zhou, K. (1991). Review of LFTs, LMIs, and mu. In *[1991] Proceedings of the 30th IEEE Conference on Decision and Control*. IEEE. doi:10.1109/cdc.1991.261572.

Gahinet, P. and Apkarian, P. (1994). A linear matrix inequality approach toH∞ control. *International Journal of Robust and Nonlinear Control*, 4(4), 421–448. doi:10.1002/rnc.4590040403.

Glover, K. and Doyle, J.C. (1988). State-space formulae for all stabilizing controllers that satisfy an h∞-norm bound and relations to relations to risk sensitivity. *Systems & Control Letters*, 11(3), 167–172. doi:10.1016/0167-6911(88)90055-2.

Knoblauch, M., Saussie, D., and Berard, C. (2012). Structured h_∞ control for a launch vehicle. In *2012 American Control Conference (ACC)*. IEEE. doi:10.1109/acc.2012.6315181.

Marwege, A., Riehmer, J., Klevanski, J., Gulhan, A., Ecker, T., Reimann, B., and Dumont, E. (2019). First wind tunnel data of callisto - reusable vtvl launcher first stage demonstrator. doi:10.13009/EUCASS2019-350.

Navarro-Tapia, D. (2019). *Robust and Adaptive TVC Control Design Approaches for the VEGA Launcher*. Ph.D. thesis, University of Bristol.

Navarro-Tapia, D., Marcos, A., Simplício, P., Bennani, S., and Roux, C. (2019). Legacy recovery and robust augmentation structured design for the VEGA launcher. *International Journal of Robust and Nonlinear Control*, 29(11), 3363–3388. doi:10.1002/rnc.4557.

Rocket Lab (2021). Neutron rocket development update. Retrieval Date: 09-Dec-2021.

Sagliano, M., Tsukamoto, T., Heidecker, A., Hernández, J.M., Farí, S., Schlotterer, M., Woicke, S., Seelbinder, D., Ishimoto, S., and Dumont, E. (2021). Robust control for reusable rockets via structured h-infinity synthesis. In *11th International ESA Conference on Guidance, Navigation & Control Systems*.

Simplicio, P., Marcos, A., and Bennani, S. (2019). New control functionalities for launcher load relief in ascent and descent flight. *8th European Conference for Aeronautics and Aerospace Sciences (EUCASS)*. doi:10.13009/EUCASS2019-275.

space.com (2015). Wow! spacex lands orbital rocket successfully in historic first. Retrieval Date: 09-Mar-2020.

Werner, H. (2014). Optimal and robust control. Technical report, Technische Universität Hamburg-Harburg. Retrieval Date: 03-March-2020.

Wie, B., Du, W., and Whorton, M. (2008). Analysis and design of launch vehicle flight control systems. In *AIAA Guidance, Navigation and Control Conference and Exhibit*. American Institute of Aeronautics and Astronautics. doi:10.2514/6.2008-6291.